Article

Linear and Nonlinear Reduced Order Models for Sloshing for Aeroelastic Stability and Response Predictions

Marco Pizzoli †, **Francesco Saltari** † and **Franco Mastroddi** *

Department of Mechanical and Aerospace Engineering, Sapienza University of Rome, Via Eudossiana 18, 00184 Rome, Italy

* Correspondence: franco.mastroddi@uniroma1.it

† These authors contributed equally to this work.

Abstract: This paper makes use of sloshing reduced-order models to investigate the effects of sloshing dynamics on aeroelastic stability and response of flying wing structure. More specifically, a linear frequency-domain operator derived by an equivalent mechanical model is used to model lateral (linear) sloshing dynamics whereas data-driven neural-networks are used to model the vertical (nonlinear) sloshing dynamics. These models are integrated into a formulation that accounts for both the rigid and flexible behavior of aircraft. A time domain representation of the unsteady aerodynamics is achieved by rational function approximation of the fully unsteady aerodynamics obtained via the doublet lattice method. The case study consists of the so called Body Freedom Flutter research model in two different configurations with one or two tanks partially filled with liquid with a mass comprising 25% of the aircraft structure. The results show that linear sloshing dynamics are able to change the stability margin of the aircraft in addition to having non-negligible effects on rigid body dynamics. On the other hand, vertical sloshing acts as a nonlinear damper and eventually provides limit cycle oscillations after flutter onset.

Keywords: flexible aircraft; aeroelasticity; linear and nonlinear sloshing; equivalent mechanical models; neural networks

1. Introduction

Aircraft are generally subjected to a wide range of loads during flight and ground operations that cause significant deformation of the wings, especially during the most severe loading phases. This can lead to sloshing of the fuel stowed in the wing tanks, whose weight is comparable to that of the structural components. The interaction between the fuel dynamics and the structure of an aircraft can in turn influence its performance, affecting both stability and response to external loads. This work is framed within the H2020 project SLOshing Wing Dynamics (SLOWD) (Ref. [1]), which studies fuel sloshing as a method to reduce loads in aircraft wings by increasing effective damping. The aim is to investigate the effects of linear and nonlinear sloshing on the stability and response of an aircraft, using reduced-order models (ROMs) capable of reproducing the forces induced by the fuel motion. The linear sloshing detailed in this analysis occurs during rotations or lateral motions of the tank. In aeronautical applications, the anticipated onset of flutter instability can arise due to the coupling between the sloshing waves generated by the structural motion and structural dynamics. Studies on the effects of lateral sloshing on the aeroelastic behaviour of aircraft can be found in Ref. [2], where the lateral sloshing is modelled via the mass-spring-damper mechanical model, in [3] where an hydroelastic added-mass model is used, in [4] where a linearized frequency domain (LFD) is employed, and in [5] where an Equivalent Mechanical Model for sloshing is used by demonstrating the effect on aeroelastic and flight mechanics stability as well. The reduced-order model used to describe linear sloshing in this work relies on the analytical formulation provided in Ref. [6] and its further

development in Ref. [7], according to which a realistic representation of linearised liquid dynamics inside containers with simplified geometry can be approximated by an equivalent mechanical model, whose parameters can be suitably related with the physical quantities obtained from the linearised potential flow theory (Ref. [8]). Nonlinear vertical sloshing, on the other hand, represents a phenomenon caused by accelerations perpendicular to the liquid free surface. Rather than providing a coupling between the dynamics of the free surface and the rest of the system, vertical sloshing can be regarded as a kind of energy sink. For small tank vertical accelerations, the free surface tends to remain flat. As the amplitude of the oscillations increases, symmetrical standing waves appear, while for vertical accelerations greater than the acceleration of gravity, the system shifts into Rayleigh–Taylor instabilities (Ref. [9]), which may determine a turbulent flow regime inside the cavity. The impacts of the liquid with the tank ceiling following free surface fragmentation cause additional dissipation of energy (see Ref. [10] for an energy-dissipated analysis via volume of fluid approach and Refs. [11–13] via Smoothed-Particle Hydrodynamics (SPH) approach as well), in which the overall balance of elastic potential energy and fluid energy leads to a noticeable increase in the effective damping of structural motion (Refs. [14,15]). In harmonic motion, this damping behavior depends on the amplitude and frequency of tank oscillations as emphasized in Refs. [16,17] via numerical simulation and experimental tests. In general, coupling between the tank structural dynamics and fluid sloshing can be solved by exploiting multi-physics interface tools (Ref. [18,19]) that couple structural finite element solvers with sloshing CFD solvers based on volume-of-fluid (Ref. [20,21]) or SPH models (Ref. [22]).

Reference [23] studied the aeroelastic response of a wing by means of the so-called *bouncing ball* reduced-order model, in which sloshing performances were characterised as a function of speed and gust intensity. The bouncing ball model provides a quick and effective way of describing this complex phenomenon (Ref. [24]), but fails in accurately representing the fluid dissipative capacity at different amplitudes and frequencies [25].

Regarding the study of vertical sloshing, a neural-network-based nonlinear ROM was generated for the wing model prototype based on the approach described in Ref. [25]. An artificial neural network (ANN) is an effective tool for reproducing the dynamic behaviour of unknown nonlinear systems (Ref. [26]). Based on time series generated by a scaled experiment, the vertical sloshing ROM is built using a nonlinear finite impulse response (NFIR) network model (see Ref. [16]). The model scaling procedure introduced in Ref. [25] is employed to extend the use of the identified ROM to applications with different tank sizes.

The final perspective offered in the present work is the integration of both linear and nonlinear sloshing ROMs into a flexible aircraft model, where flight dynamics and aeroelasticity are involved. It is assumed that sloshing forces can be decomposed into a lateral part with linearised behavior and a vertical part with extremely nonlinear behavior by neglecting their mutual interactions. The present work mainly relies on the approach described in [27], where a fully coupled equation of the aircraft motion was derived by assuming practical mean axes (PMA) constraints. The structure is modelled using the finite element method (FEM), whereas the doublet lattice method (DLM) is used to describe the unsteady aerodynamics (see Ref. [28]). Using the rational polynomial function approximation, the unsteady aerodynamics are recast into a pure differential expression that requires a new set of aerodynamic state-space variables (see Ref. [29]). The integration of linear sloshing, described by means of an EMM, introduces additional state variables (analogous to aerodynamics), thus representing latero-rotational sloshing dynamics. Vertical sloshing interacts with the aeroelastic model by providing a nonlinear force contribution that depends on the vertical excitation of the aircraft tanks. The combined effect of linear and nonlinear sloshing dynamics is modelled by adding the two contributions that they provide to the system. The reference aircraft is the Body Freedom Flutter (BFF) (whose model is proposed in Ref. [30]) and a flutter suppression strategy also proposed in Ref. [31]) in two different cases or configurations. The first contains only one tank that is partially filled with a low-density liquid and is placed beneath the aircraft's center of mass whereas the

second case has two rectangular tanks symmetrically placed beneath the wings. Sloshing and frozen mass (in which liquid is simply a ballast) models are compared to quantify the sloshing effects on aircraft aeroelastic behavior. Stability analyses show how the coupling between linear sloshing, aircraft aeroelasticity, and flight dynamics contribute to modification of the overall aircraft stability scenario. Nonlinear response aeroelastic analyses demonstrate that dynamic load alleviation is achieved when vertical (nonlinear) sloshing is also included in the overall aeroelastic model. Moreover, limit cycle oscillations arise after the onset of flutter due to the dissipative characteristics of vertical sloshing.

The paper is organised as follows. The flexible aircraft and sloshing modeling are introduced in Section 2. The case studies are introduced in Section 3 whilst the stability analysis and aeroelastic responses are illustrated in Section 4, comparing the performance of sloshing models with the frozen configuration. Finally, concluding remarks are provided at the end of the paper.

2. Flexible Aircraft with Sloshing Integrated Modeling

This work aims to include the linear and nonlinear dynamics of sloshing within an integrated flexible aircraft formulation in order to study the effects in terms of aeroelastic response. The present modeling is based on the formulation presented in Refs. [5,27], in which the rigid body degrees of freedom are associated with the so-called practical mean axes (PMAs), characterised by having the PMA frame origin located at the instantaneous center of mass and orientation of the principal axes invariant with respect to the deformations.

The linearised elastic deflections are described as a combination of unconstrained aircraft mode shapes in the PMAs thus relaxing the inertial formulation.

The equations of motion for the conservation of momentum and angular momentum and the equations of the structural dynamics are given by:

$$
\begin{aligned}
m\frac{d\mathbf{v}_{\mathrm{G}}}{dt} &= \mathbf{f}_{\mathrm{T}} \\
\frac{d\mathbf{h}_{\mathrm{G}}}{dt} &= \mathbf{m}_{\mathrm{G}} \\
m_n\ddot{q}_n + k_n q_n &= f_n \qquad n = 1,\dots,N_m
\end{aligned}
\tag{1}
$$

where $\mathbf{v}_{\mathrm{G}}$ and $\mathbf{h}_{\mathrm{G}}$ are the center of mass velocity and the angular momentum, respectively, m is the total mass, $\mathbf{f}_{\mathrm{T}}$ and $\mathbf{m}_{\mathrm{G}}$ are the aerodynamic force and moment, respectively, whereas q_n denotes the n-th modal coordinate, m_n, k_n, and f_n are the n-th modal mass, stiffness and generalized aerodynamic force and N_m is the number of flexible modes included in the analysis. The equations of motion (1) are then recast with respect to a body frame of reference and linearised around a level flight aeroelastic trim condition:

$$
\begin{aligned}
m\frac{d\mathbf{v}_{\mathrm{G}}}{dt} = m\dot{\mathbf{v}}_{\mathrm{G}} + \boldsymbol{\omega} \times \mathbf{v}_{\mathrm{G}} &\approx m\Delta\dot{\mathbf{v}}_{\mathrm{G}} - \mathbf{v}_{\mathrm{G}_e} \times \Delta\boldsymbol{\omega} = \Delta\mathbf{f}_{\mathrm{T}} \\
\frac{d\mathbf{h}_{\mathrm{G}}}{dt} = \frac{d\mathbf{J}\boldsymbol{\omega}}{dt} + \boldsymbol{\omega} \times \mathbf{J}\boldsymbol{\omega} &\approx \mathbf{J}\Delta\dot{\boldsymbol{\omega}} = \Delta\mathbf{m}_{\mathrm{G}} \\
m_n\Delta\ddot{q}_n + k_n\Delta q_n &= \Delta f_n \qquad n = 1,\dots,N_m
\end{aligned}
\tag{2}
$$

where $\mathbf{J}$ is the inertia tensor, and $\boldsymbol{\omega}$ is the angular velocity. It is worth noting that, if a linearization around a trimmed straight flight solution is performed, the inertial coupling terms in Ref. [27] can be neglected.

The variables associated to second-order dynamics are grouped in the following vector:

$$
\Delta\eta = \left\{ \Delta\mathbf{x}_{\mathrm{G}}^{\mathrm{T}}, \Delta\Theta^{\mathrm{T}}, \Delta\mathbf{q}^{\mathrm{T}} \right\}^{\mathrm{T}}
\tag{3}
$$

where

$$
\begin{aligned}
\Delta x_G &= \{\Delta x_G, \Delta y_G, \Delta z_G\}^T \\
\Delta \Theta &= \{\Delta \phi, \Delta \theta, \Delta \psi\}^T
\end{aligned}
\tag{4}
$$

are, respectively, the perturbation vectors of the center of mass coordinates in the inertial frame of reference and of the Euler angles. Moreover, the perturbation vector of the modal coordinates is given by

$$
\Delta q = \{\Delta q_1, \dots, \Delta q_{N_m}\}^T
\tag{5}
$$

Nevertheless, the equations of motion of the aircraft are expressed in a non inertial frame of reference. Indeed, the following vector is defined

$$
\Delta \nu = \left\{ \Delta v_G^T, \Delta \omega^T, \Delta \dot{q}^T \right\}^T
\tag{6}
$$

where $\Delta v_G = \{\Delta u, \Delta v, \Delta w\}^T$ and $\Delta \omega = \{\Delta p, \Delta q, \Delta r\}^T$ are the translational and angular velocities in the PMAs coordinate system, respectively. The linearised relation between $\Delta \eta$ in Eq. (6) and $\Delta \nu$ is expressed as

$$
\Delta \dot{\eta} = \Delta \nu + T_1^* \Delta \eta
\tag{7}
$$

with

$$
T_1^* = \begin{bmatrix} 0_{3\times3} & -\hat{V}_{G_e} & 0_{3\times N_m} \\ 0_{3\times3} & 0_{3\times3} & 0_{3\times N_m} \\ 0_{N_m\times3} & 0_{N_m\times3} & 0_{N_m\times N_m} \end{bmatrix}, \quad \hat{V}_{G_e} = \begin{bmatrix} 0 & 0 & 0 \\ 0 & 0 & -U_\infty \\ 0 & U_\infty & 0 \end{bmatrix}
\tag{8}
$$

where $0_{\bullet\times\bullet}$ are zero matrices with suitable number of rows and columns. Equation (8) allows one to highlight the link between the variables expressed in the PMAs and those defined in the inertial reference system (being T_1^* a square matrix with dimension $N = 6 + N_m$). Taking into account the external action of aerodynamics and sloshing dynamics, the system of Equation (2) can be rewritten as follows:

$$
M \Delta \dot{\nu} + D \Delta \nu + K \Delta \eta = e + g + f^{(ext)}
\tag{9}
$$

where M, D and K are, respectively, the modal mass, damping and stiffness (diagonal) matrices of the flexible aircraft, whereas $e = [e_1, e_2, \dots, e_N]^T$ and $g = [g_1, g_2, \dots, g_N]^T$ are, respectively, the generalized *aerodynamic* and *sloshing* forces induced by the aircraft motion. These forces are generally defined as a projection of physical applied force fields (aerodynamics and sloshing) on the assumed rigid and flexible mode shapes. In the present paper, the wing body is assumed to be locally rigid in the neighborhood of the tank (see Refs. [16,32]) and therefore, the force-field projection becomes a scalar product (see later Equation (20)). The $f^{(ext)}$ is the vector of the current external forcing terms such as the gust excitation. A description of the aircraft motion in the PMA non-inertial reference requires accounting for the projection of the weight force on the aircraft body reference. Under the assumption of small perturbations with respect to the trimmed configuration, such a contribution was modelled as an additional stiffness term included inside K.

The generalised aerodynamic force vector is generally computed as a function of the reduced frequency $k = \omega b / U_\infty$ (with b semi-chord and U_∞ free stream velocity) and Mach number M_∞ domain (see Ref. [28]) as:

$$
\tilde{e} = q_D Q(k, M_\infty) \Delta \tilde{\eta}
\tag{10}
$$

where $Q(k, M_\infty)$ is the generalised aerodynamic forces matrix, q_D is the dynamic pressure and the symbol $\tilde{\ }$ is used to represent the Laplace/Fourier transforms. For a fixed value of

M_∞, the following rational function approximation for the unsteady aerodynamics can be considered (Ref. [29])

$$Q(k) \approx A_0 + jkA_1 - k^2A_2 + jkC\left(jkI + P\right)^{-1}B \tag{11}$$

Introducing the aerodynamic states vector a and exploiting the definition of inverse Fourier transform, the aerodynamic forces can be recast in time domain as:

$$e = q_D A_0 \Delta\eta + q_D \frac{b}{U_\infty} A_1 \Delta v + q_D (\frac{b}{U_\infty})^2 A_2 \Delta\dot{v} + q_D C a \tag{12}$$

$$\dot{a} = \frac{U_\infty}{b} P a + B \Delta v \tag{13}$$

In this work, the effects of two different sloshing dynamics are considered. The first is present when small lateral displacements and rotations are imposed on the tanks. In these cases, the dynamics can be considered linear (Ref. [32]) and give rise to sloshing generalised loads referred to as g_l. The second is nonlinear, and its action g_{nl} is triggered by large vertical perturbations imposed on the tanks.

Thus, the generalised sloshing forces vector g is constructed as a sum of contributions $g^{(i)}$ of individual tanks:

$$g = \sum_{i=1}^{N_T} g^{(i)} = \sum_{i=1}^{N_T} \left(g_l^{(i)} + g_{nl}^{(i)} \right) \tag{14}$$

with N_T denoting the number of tanks.

The linear contribution arises from the presence of lateral standing waves and is modelled using equivalent mechanical models that allow exertion of the force and moment by the liquid, following the application of a small lateral displacement or rotation. The lateral sloshing forces for each tank in the Laplace domain are expressed by means of a generalised sloshing forces matrix $G(s)^{(i)}$ as

$$\tilde{g}_l^{(i)} = \bar{G}(s)^{(i)}\Delta\tilde{\eta} \tag{15}$$

Reference [5] provides a formulation of the linear lateral sloshing forces based on the analytical model (Ref. [6]), and accordingly, the generalized sloshing forces can be recast as follows:

$$\tilde{g}_l^{(i)} = s^2 \bar{A}_s^{(i)} \Delta\tilde{\eta} + \left(s^2\bar{B}_s^{(i)} + \bar{C}_s^{(i)} \right) \tilde{r}^{(i)} \tag{16}$$

where the linear sloshing modal coordinates $\tilde{r}^{(i)}$ are introduced as

$$\tilde{r}^{(i)} = \left[\left(s^2I + sD_s^{(i)} + \Omega_s^{2(i)} \right)^{-1} \left(s^2 \bar{B}_s^{(i)} + \bar{C}_s^{(i)} \right)^{\mathsf{T}} \right]\Delta\tilde{\eta} \tag{17}$$

and $\bar{A}_s^{(i)}, \bar{B}_s^{(i)}, \bar{C}_s^{(i)}, D_s^{(i)}$ and $\Omega_s^{2(i)}$ are the coefficient matrices of the lateral sloshing operator. It is worth mentioning that $\Omega_s^{2(i)}$ and $\bar{D}_s^{(i)}$ are, respectively, the natural frequency and damping modal coefficient matrices of the considered linear sloshing modes. The same representation of the sloshing force can be achieved by a linear frequency-domain approach as in Ref. [4,32]. The inverse Laplace transform of Equations (15) and (17) leads to

$$g^{(i)} = \bar{A}_s^{(i)}\Delta\ddot{\eta} + \bar{B}_s^{(i)}\ddot{r} + \bar{C}_s^{(i)}r^{(i)} \tag{18}$$

$$\ddot{r}^{(i)} + D_s^{(i)}\dot{r}^{(i)} + \Omega_s^{2(i)} r^{(i)} = \bar{B}_s^{(i)\mathsf{T}} \Delta\ddot{\eta} + \bar{C}_s^{(i)\mathsf{T}} \Delta\eta \tag{19}$$

in which the second-order dynamics of the sloshing modal coordinates are highlighted.

The nonlinear force contribution is instead related to the so-called *dynamic sloshing force* $\Delta f_{S_z}^{(i)}$ given by the relative acceleration of the liquid particles with respect to the *i-th* tank

non-inertial frame (see Ref. [25]). The *n-th* component of $g_{nl}^{(i)}$ is the projection (following the approximation previously discussed after Equation (9)) of the sloshing dynamic force on each *n-th* rigid and elastic modal shape $\boldsymbol{\psi}_n$ as:

$$g_{nl_n}^{(i)} = \boldsymbol{\psi}_n(\mathbf{x}_{T_i}) \cdot \mathbf{i}_3 \, \Delta f_{S_z}^{(i)} \tag{20}$$

where $\mathbf{x}_{T_i}$ is the geometrical center of the *i-th* tank, $\mathbf{i}_3$ is the vertical unit vector of the inertial frame of reference and $\boldsymbol{\psi}_n(\mathbf{x}_{T_i})$ is the *n-th* mode shape evaluated in the *i-th* tank center.

The formulation is implemented in Simulink®, as illustrated in Figure 1, creating a numerical model combining a purely differential linear problem describing flight dynamics, aeroelasticity and linear sloshing, and a data-driven model representing nonlinear vertical sloshing dynamics.
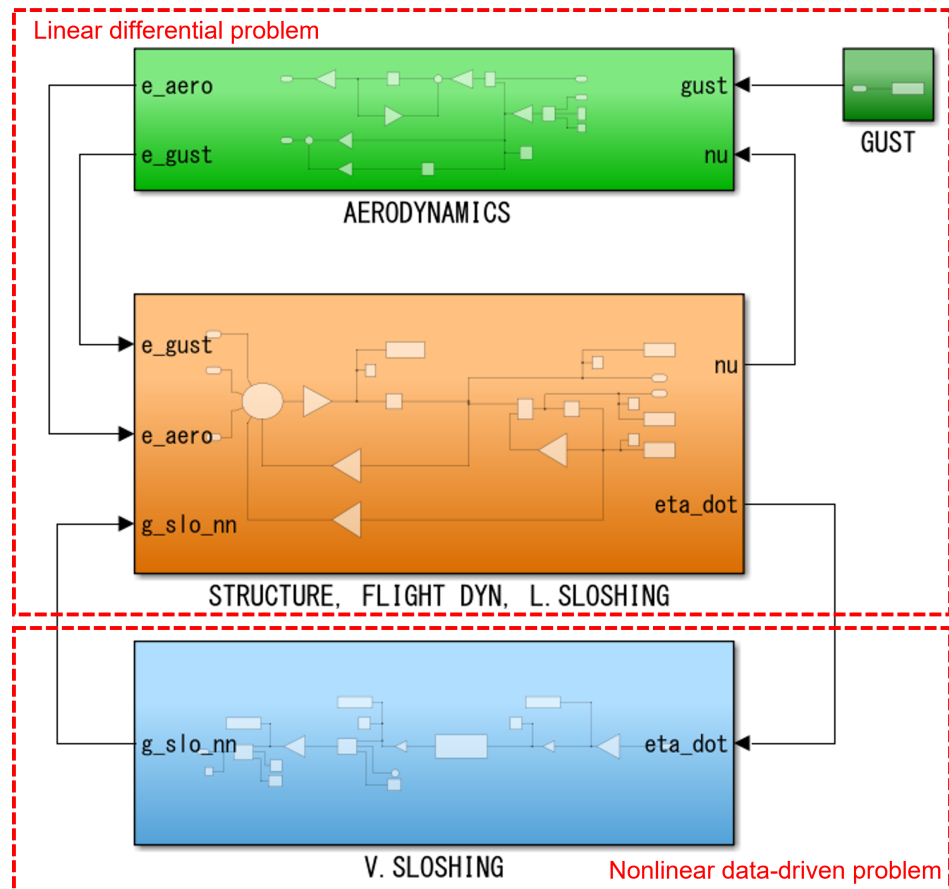

Figure 1. Flexible aircraft with linear and nonlinear sloshing modeling in Simulink®.

Concerning the nonlinear sloshing block, Refs. [25,33] provide further details about nonlinear reduced-order modeling based on a neural network driven by experimental data obtained with a suitable scaled tank. The neural network receives the tank's vertical velocity expressed in the inertial frame of reference and provides an estimate of the already defined dynamic sloshing force Δf_{S_z}. The considered neural-network-based dynamical model is a Nonlinear Finite Impulse Response (NN-NFIR) model represented in Figure 2, whose hyper-parameters are the same as those introduced in Ref. [25].
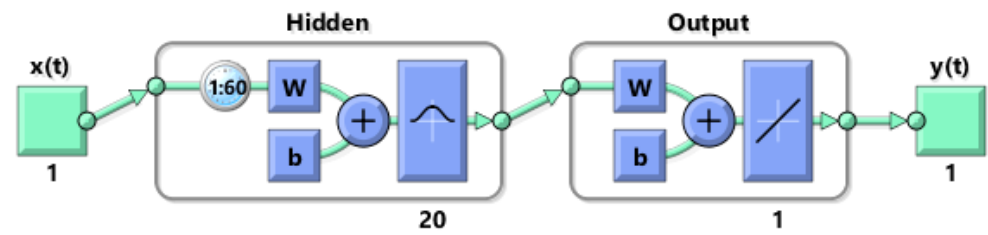
Figure 2. Time-Delay Neural Network flowchart

3. Case Studies

The case studies analysed in this work are based on the finite element model (FEM) of the Body-Freedom-Flutter (BFF), an unmanned flying-wing research aircraft model of total mass $M = 5.44$ Kg (without tanks), half-chord $b = 0.2$ m, wingspan equal to 3.048 m and projected wing surface area equal to 1.084 m^2. The model takes its name from its flutter mode involving both the vibrations and rigid-body motion of the aircraft (Ref. [30]). The first six flexible modes, with their respective frequencies, are shown in Figure 3.
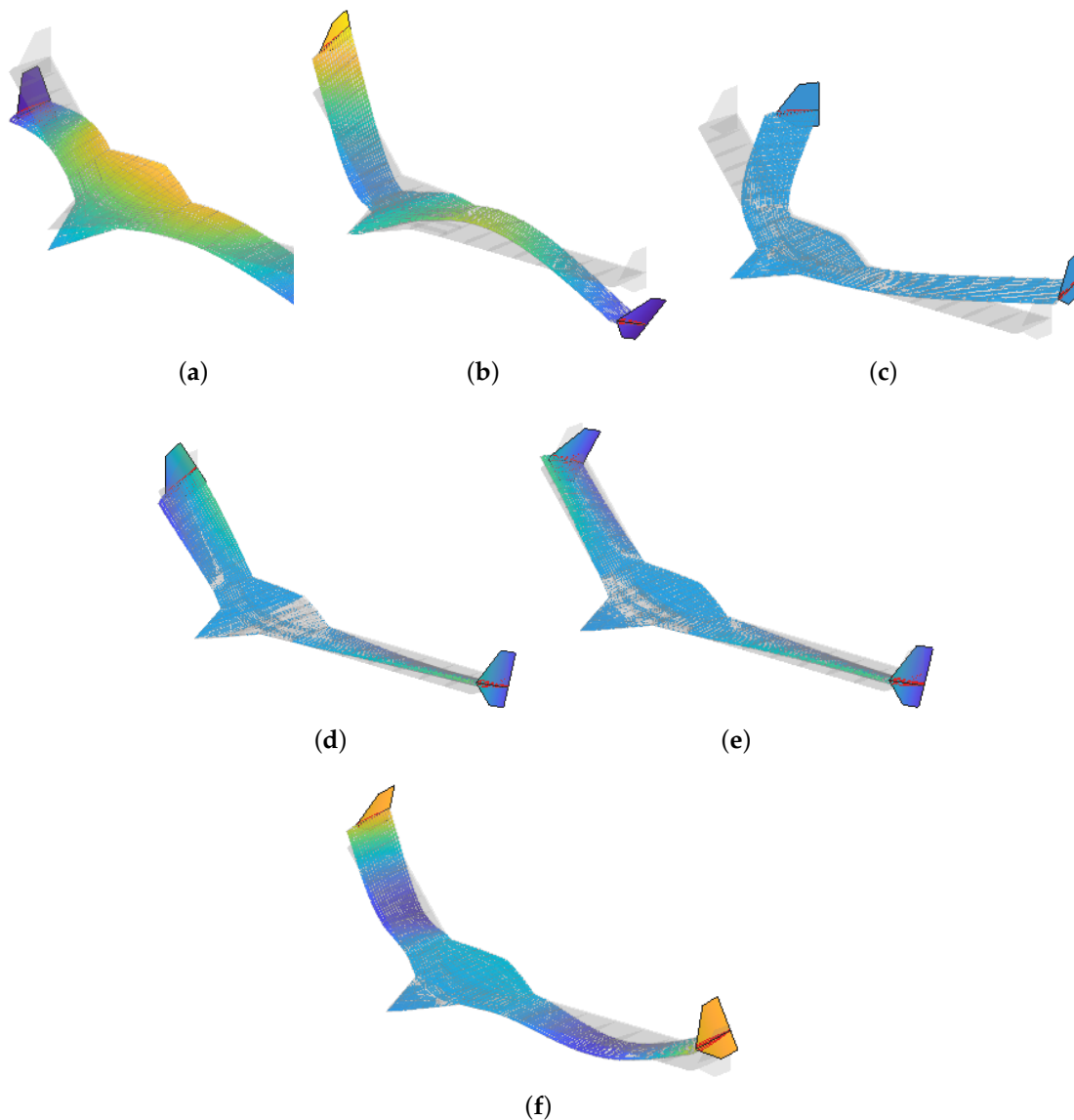
Figure 3. Elastic mode shapes of the model. Captions indicate their natural frequencies. (**a**) $f_1 = 5.83$ Hz. (**b**) $f_2 = 8.83$ Hz. (**c**) $f_3 = 13.45$ Hz. (**d**) $f_4 = 19.82$ Hz. (**e**) $f_5 = 20.09$ Hz. (**f**) $f_6 = 23.72$ Hz.

The effects of sloshing dynamics on the aircraft are investigated in two different configurations, one with a single tank under the center of mass (see Figure 4) and the other with two tanks symmetrically placed under the wings (see Figure 5). The geometric dimensions of the tank in Case study 1 (half-filled with a liquid with a density of $\rho = 650\,\text{kg/m}^3$) are listed in Table 1 and are such that the total mass of liquid contained accounts for 25% of the structural mass of the aircraft. The configuration in Figure 4 will hereafter be denoted as Case study 1.
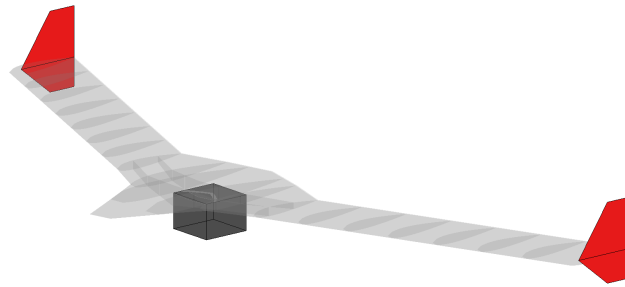
Figure 4. Configuration with one box-shaped tank placed underneath the BFF center of mass.

Table 1. Tank geometry—Case study 1.

Parameter	Value (m)
side in direction x	0.18
side in direction y	0.18
h (height)	0.13
h_f (filling level 50%)	0.065

In the present analysis, three sloshing modes were considered in a linear lateral analysis for both the dynamics along x and y (in plane dimensions). The natural frequencies of linear sloshing are reported in Table 2 (when the tank is detached from the structure).

Table 2. Linear sloshing natural frequencies—Case study 1.

Mode Number	Direction	Frequency (rad/s)
1,2	x, y	11.80
3,4	x, y	22.64
5,6	x, y	29.26

Case study 2 was realised by considering two tanks created by halving the tank shown in Table 1 in the y-direction to ensure that the same amount of liquid was carried by the aircraft (see Table 3). The natural frequencies of sloshing in this case differ depending on the planar direction of the tanks under consideration, as can be seen in Table 4. This implies the presence of three modal coordinates describing the linear sloshing, referred to as $r_1^{(i)}$, $r_2^{(i)}$ and $r_3^{(i)}$, for both tanks.

From the point of view of the FEM solver, the presence of the tanks in both configurations was managed by creating a node located in their geometrical center, linked to the body of the aircraft by means of the rigid body element (RBE). A concentrated mass is considered to represent the structural mass of the tanks.

On the other hand, the small disturbance unsteady aerodynamics is modeled via the Doublet Lattice Method (DLM) available in MSC Nastran for unsteady linear aeroelastic analysis (Ref. [28]). As can be seen in Figure 1, linear sloshing was included in the same block as the structural and flight dynamics model of the aircraft. Indeed, combining Equations (9), (14) and (16), it becomes possible to obtain an augmented model with additional modal variables represented precisely by the added state-space vector r.
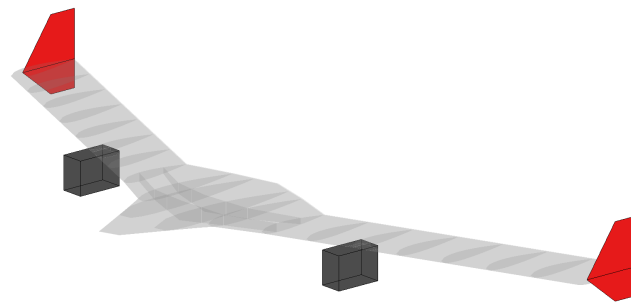
Figure 5. Configuration with two box-shaped tanks placed under the BFF wings.

Table 3. Tank geometry—Case study 2.

Parameter	Value (m)
side in direction x	0.18
side in direction y	0.09
h (height)	0.13
h_f (filling level 50%)	0.065

Table 4. Linear sloshing natural frequencies—Case study 2.

Mode Number	Direction	Frequency (rad/s)
1	x	11.80
2	y	18.31
3	x	22.64
4	y	32.05
5	x	29.26
6	y	41.38

4. Aeroelastic Stability and Response Analyses

This section presents the stability and response analyses performed for the two configurations presented in Section 3, highlighting the effects of lateral (linear) and vertical (nonlinear) sloshing dynamics regarding cases where the liquid is frozen (r = 0 and $\Delta f_{S_z} = 0$). The linearised aeroelastic system of the two case studies is used to evaluate the stability scenario of the aircraft between $13\,\mathrm{m/s}$ and $30\,\mathrm{m/s}$ considering incompressible and sea-level flow conditions. On the other hand, gust response analyses at different velocities in the neighbourhood of the flutter speed are performed to investigate the role of sloshing in damping aircraft vibrations. Specifically, the following standard gust profile is considered for both case studies:

$$w_g(t) = \begin{cases} \frac{1}{2} w_{g_a} \left[1 - \cos\left(\frac{2\pi U_\infty t}{L_g} \right) \right] & \text{if} \quad 0 < t < \frac{L_g}{U_\infty} \\ 0 & \text{if} \quad t \geq \frac{L_g}{U_\infty} \end{cases} \tag{21}$$

where w_{g_a} is the gust amplitude and b the chord length. The set value of the gust length is $L_g = 25\,b$. Spatially, the gust is assumed to be constant throughout the wing domain. Four models will be compared for both case studies, namely the *frozen fuel* model, the *lateral (linear) sloshing* model, the *vertical (nonlinear) sloshing* model, and the *full sloshing* model, in which both forms of the sloshing considered in this analysis are accounted for.

4.1. Test Case 1

The stability scenario of the aircraft model in the frozen liquid configuration (blue diamonds) is compared in Figure 6 with the lateral sloshing considered in the formulation

(red squares). Figure 6b highlights the additional poles representing linear sloshing dynamics, along with rigid-body dynamics. Lateral sloshing slightly worsens the stability of the aircraft with respect to the frozen fuel case. In fact, the flutter speed U_F slightly decreases from 18.95 m/s to 18.8 m/s. This corresponds to a slight change in the critical frequency ω_F, which increases from 23.53 rad/s (3.74 Hz) to 23.82 rad/s (3.79 Hz). In both configurations, the critical mode occurs due to the coupling between the *short period* mode and the first vibration mode. The crossing of the imaginary axis occurs with the pole originating from the branch of the first mode (see Figure 6a). Furthermore, sloshing dynamics have a non-negligible effect on *dutch roll* and *phugoid*, rendering the latter less stable and very close to the imaginary axis. On the other hand, the higher frequency poles are only minimally affected and show no particular changes compared to the frozen case.
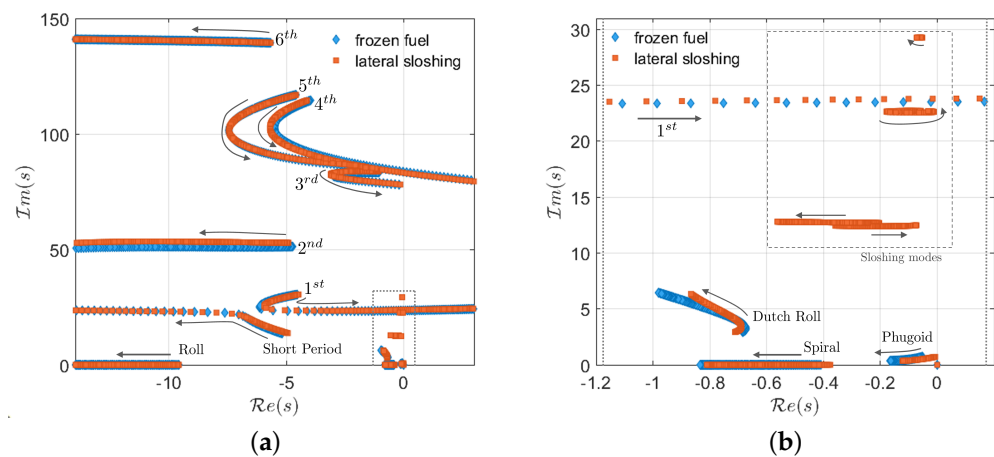

Figure 6. Root locus with linear sloshing—Test Case 1. (**a**) Root locus of the integrated system. (**b**) Focus on the rigid body and sloshing modes.

　　Two different flight conditions are considered for gust response analysis, that is $U_\infty = 18$ m/s (i.e., before the flutter speed of the linear sloshing and the frozen fuel models), and $U_\infty = 19.35$ m/s (after flutter onset). Moreover, dependency of the vertical-sloshing-induced damping by the response magnitude is investigated by taking into account different gust amplitudes. The first analysis is performed at a free-stream velocity of $U_\infty = 18$ m/s, with a gust intensity of $w_{g_a} = 2.5$ m/s. Being slightly under pre-critical conditions (speed equal to 95% and 96% of the flutter speeds of the frozen and lateral sloshing models), the response is expected to be slightly damped. Figure 7a compares aircraft responses of the four considered models in terms of local angle of attack (AoA = $\Delta w/U_\infty$). Similarly, Figure 7b shows the comparison in terms of the response of the first dry vibration mode q_1, whose values are measured in meter units when normalised to unit displacement. A reasonable result is the ability of vertical sloshing dynamics in dampening the aeroelastic response more than that in the frozen case due to the sloshing impacts occuring in the tank. It also leads to a change in the frequency of the response, which is lower than that in the frozen case. Linear sloshing does not introduce dissipative effects into the response, but induces a slight increase in frequency (in the same manner as the critical frequency). Figure 8 shows the time trends of the nonlinear dynamic sloshing force for the vertical and full sloshing models. The forces almost overlap because the neural-network-based reduced-order model receives a similar tank velocity as input for both models. The particularly nonlinear response in the first three cycles is caused by impacts between the fluid and the tank walls. Finally, Figure 9 shows comparisons between the responses of the first two added sloshing modes (in the *x*-direction) in the linear and full sloshing models. The modes in question do not appear to be influenced by aeroelastic or rigid-body dynamics, but solely by the initial condition imposed by the external gust. The vertical sloshing effect dampens the second mode response for a few seconds, before

becoming irrelevant. Sloshing modes in the y-direction are not affected by the gust and therefore do not exhibit active dynamics.
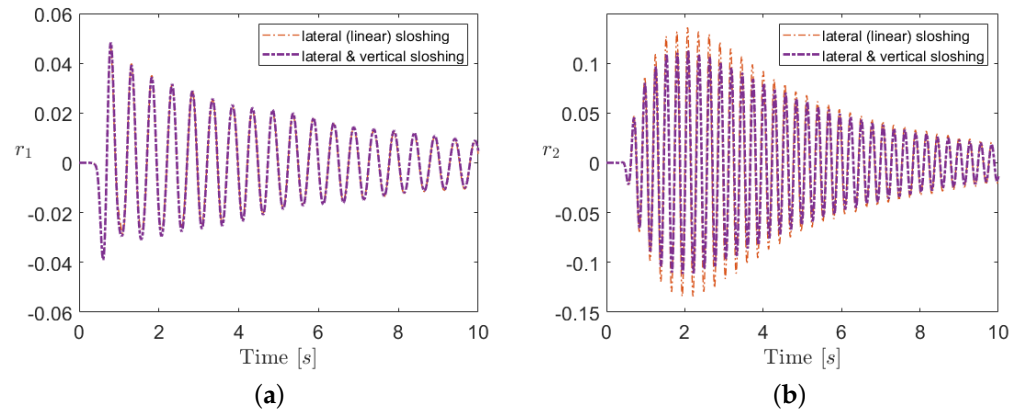

(a)

(b)
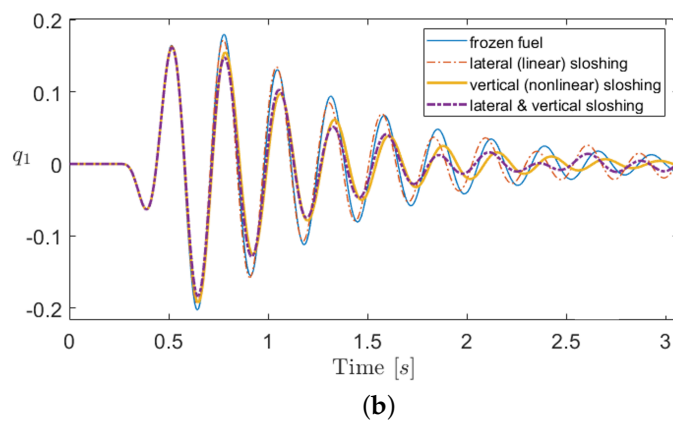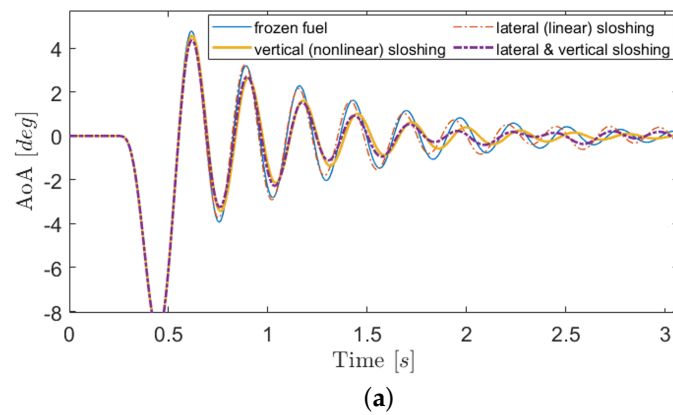
Figure 7. $U_\infty = 18\,\mathrm{m/s}$ and $w_{g_a} = 2.5\,\mathrm{m/s}$—Test Case 1. (**a**) Local angle of attack. (**b**) First structural mode.
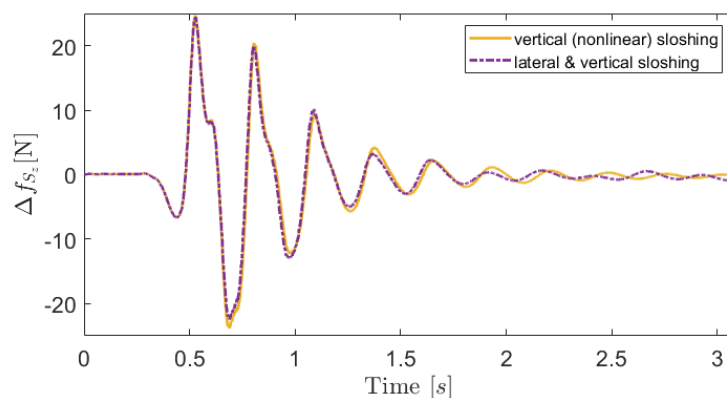

Figure 8. Dynamic sloshing force for $U_\infty = 18\,\mathrm{m/s}$ and $w_{g_a} = 2.5\,\mathrm{m/s}$—Test Case 1.

A response analysis is then performed at $U_\infty = 19.35\,\mathrm{m/s}$ in the developed flutter condition with a gust amplitude of $w_{g_a} = 0.3\,\mathrm{m/s}$. Under flutter conditions (with speeds 2% and 3% higher than flutter speeds of the frozen and lateral sloshing models, respectively), the response is expected to be unstable with the exponential envelope. The local angle of attack and the first mode responses are shown in Figure 10a,b comparing the effects that the four considered models have on the post-critical response of the flying wing. The linear sloshing model and the frozen fuel configuration results in an unstable response. In contrast, vertical sloshing helps prevent the response from growing indefinitely, favoring

the onset of limit cycle oscillations (LCOs). This behaviour is determined by the nature of the nonlinear sloshing forces, which become highly dissipative when the acceleration of the tank increases. In the case of a combined effect of the two sloshing dynamics, the oscillation amplitude is greater than that in the case of vertical sloshing alone.


Figure 9. Sloshing modes for $U_\infty = 18\,\mathrm{m/s}$ and $w_{g_a} = 2.5\,\mathrm{m/s}$—Test Case 1. (**a**) First mode (dir. x). (**b**) Second mode (dir. x).
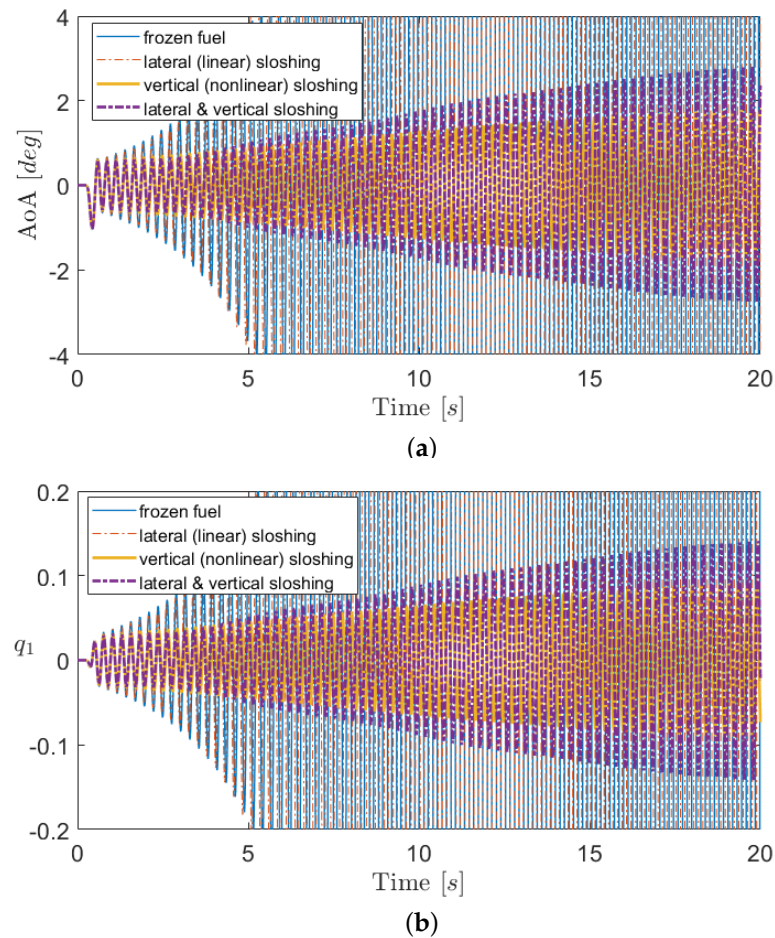
Figure 10. $U_\infty = 19.35\,\mathrm{m/s}$ and $w_{g_a} = 0.3\,\mathrm{m/s}$—Test Case 1. (**a**) Local angle of attack. (**b**) First structural mode.
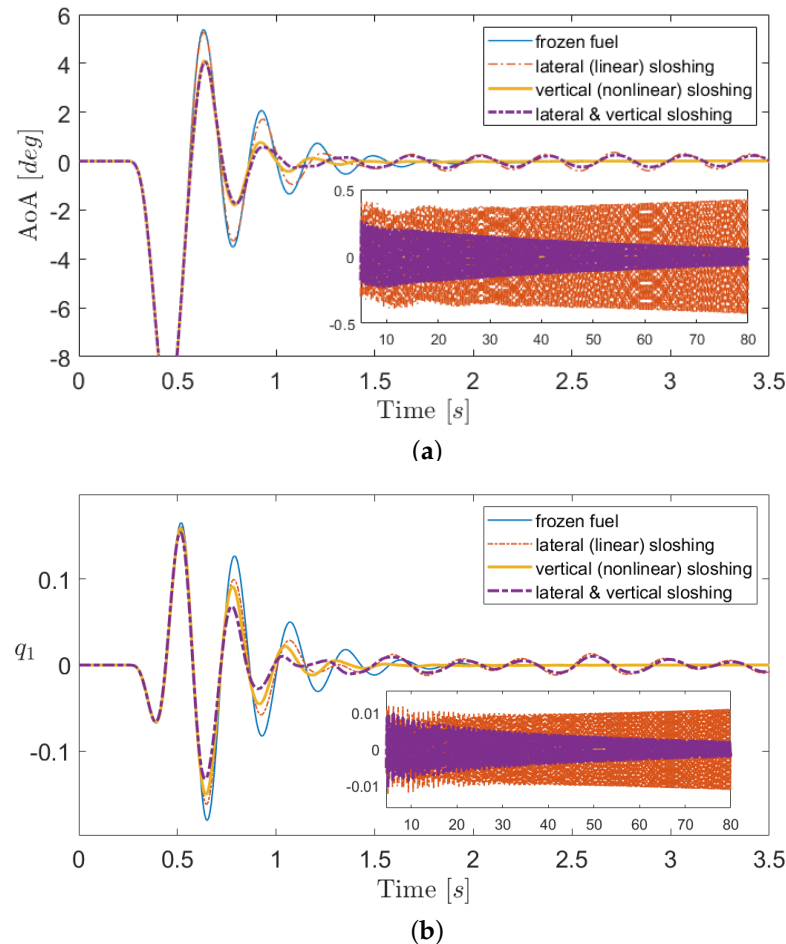
4.2. Test Case 2

Figure 11 shows the results of the stability analysis conducted for the second case study, both for the frozen model (blue diamonds) and for the linear sloshing model (red squares). The stability scenario of the frozen model is different from that of Test Case 1. In fact, to ensure the static stability of the two-tank configuration, it was necessary to place them under the wings with an offset in the longitudinal direction. Such a tank location emphasizes the coupling between the torsional mode (fourth mode) and the anti-symmetrical bending mode (second mode). For the frozen model, flutter instability occurs at $U_\infty = U_F = 20.86 \, \mathrm{m/s}$ with the branch originating from the *short period* (see Figure 11a), whereas the flutter frequency is $\omega_F = 22.7 \, \mathrm{rad/s} \, (3.61 \, \mathrm{Hz})$. The critical mode occurs due to coupling between the *short period* and *first vibration* mode. Note that the third mode becomes unstable at a flight speed of $U_\infty = 22.65 \, \mathrm{m/s}$, which corresponds to a frequency value equal to $48.22 \, \mathrm{rad/s} \, (7.67 \, \mathrm{Hz})$. Lateral sloshing introduces poles which significantly affect the aircraft dynamics. Figure 11b highlights the rigid-body dynamics and the added dynamics of linear sloshing. The latter crosses the imaginary axis at a low velocity equal to $U_\infty = 16.2 \, \mathrm{m/s}$, rendering the system slightly unstable. The presence of sloshing dynamics increases the stability of the body freedom flutter pole (short-period mode) augmenting the flutter margin to $U_\infty = 21.71 \, \mathrm{m/s} \, (\omega = 23.12 \, \mathrm{rad/s})$. However, there is also a deterioration in the stability of the third mode, which crosses the imaginary axis at a speed of $U_\infty = 20.94 \, \mathrm{m/s} \, (\omega = 49.13 \, \mathrm{rad/s})$ giving rise to a critical bending-torsional mode. Sloshing dynamics also have an impact at low frequencies, also affecting both the frequency and damping of *dutch roll* and *phugoid* .
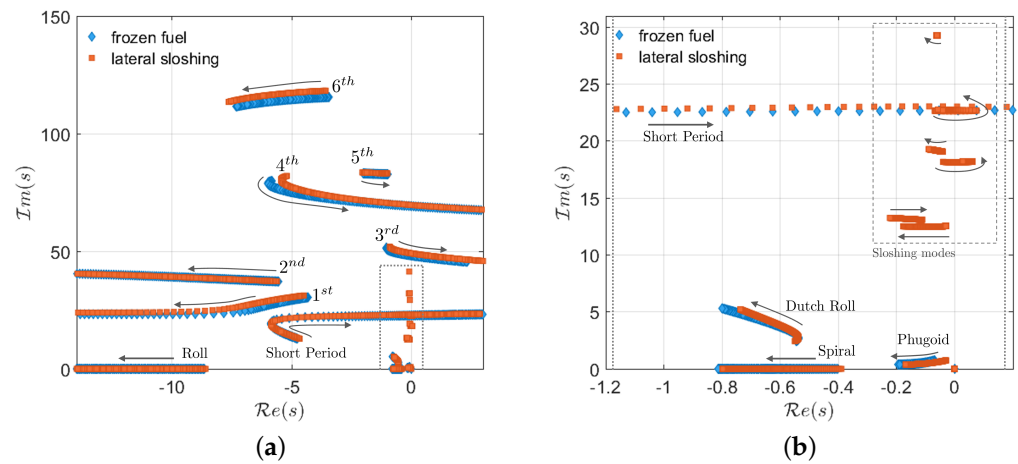
Figure 11. Root locus with linear sloshing—Test Case 2. (**a**) Root locus of the integrated system. (**b**) Focus on the rigid body and sloshing modes.

Different aeroelastic analyses are considered by varying the speed and gust amplitude. The first analysis is performed at a free-stream velocity of $U_\infty = 18 \, \mathrm{m/s}$ (speed equal to 86% and 83% of the body freedom flutter mode critical speeds of the frozen and lateral sloshing models, respectively), with a gust intensity of $w_{g_a} = 3 \, \mathrm{m/s}$. In this condition (see Figure 11b), the linear sloshing model is unstable due to the crossing of the imaginary axis by a sloshing pole, whilst the frozen fuel model remains stable. The local angle of attack and the first structural mode responses are, respectively, shown in Figure 12a,b, comparing the four different models considered. Vertical sloshing contributes to dampening of the responses of both quantities shown also providing an increase in response frequency. As can be seen from the structural response, linear sloshing provides a damping contribution, which is, however, less clear than that in the local angle of attack. This highlights the full sloshing model as the one demonstrating the most damped response for the first bending mode. The tail of the response is featured by the trigger of unstable sloshing dynamics that also bears a small effect on the structural and flight dynamics components (see inset plots

in Figure 12). Albeit very slowly, vertical sloshing succeeds in containing this instability. Increasing oscillations become unphysical as they are associated with sloshing mode. This means that when accounting for the nonlinear behaviour of lateral sloshing (not considered in this work), the dynamics will be limited in oscillation amplitudes.
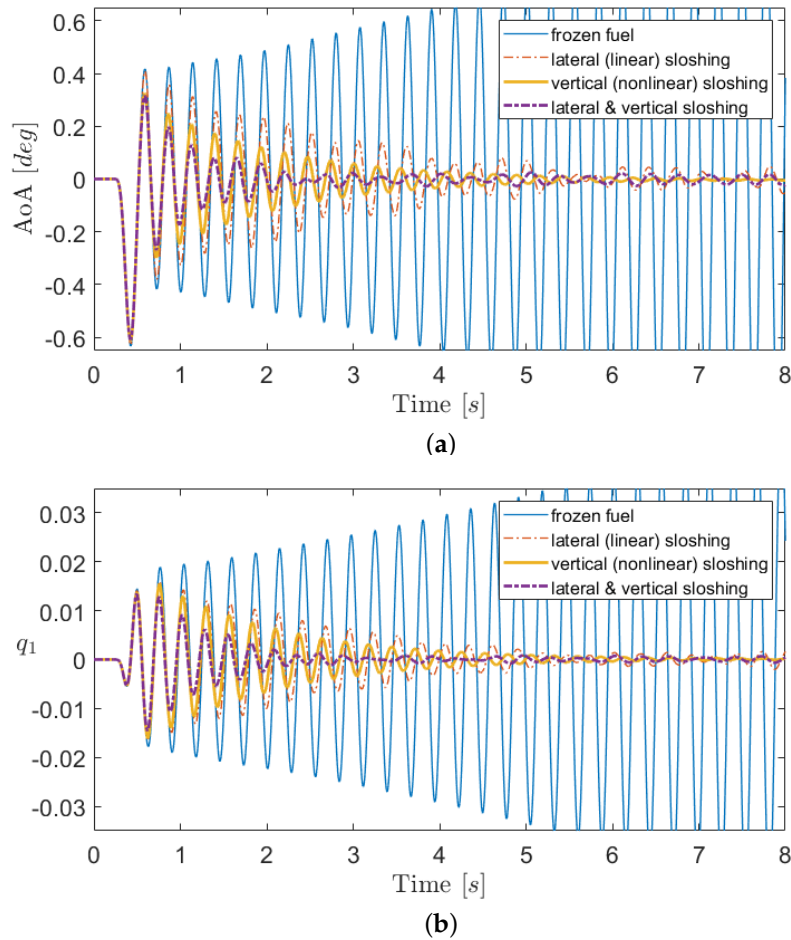

Figure 12. $U_\infty = 18\,\text{m/s}$ and $w_{g_a} = 3\,\text{m/s}$—Test Case 2. (**a**) Local angle of attack. (**b**) First structural mode.

The second gust response analysis is performed at $U_\infty = 21.1\,\text{m/s}$ (a speed 1% higher than the flutter speed of the frozen fuel model and 97% of the body freedom flutter mode critical speed of the lateral sloshing model), with a gust intensity of $w_{g_a} = 0.2\,\text{m/s}$. In this flight condition, the model with linear sloshing is unstable due to the critical bending-torsional mode. Figure 13 compares the responses of the four considered models in terms of local angle of attack and Figure 13b shows the comparison in terms of the response of the modal variable associated with the first bending mode. The frozen case results in an unstable response, whereas the case of vertical sloshing presents a damped response. The lateral sloshing model exists in an unstable condition due to the critical bending-torsional antisymmetric mode. However, the applied gust, as symmetric input, is unable to trigger this dynamics. In addition, the body freedom flutter occurs at a higher velocity and this leads to a more damped response. The addition of vertical sloshing further dampens the response of the full sloshing case.

The last analysis is performed in the body freedom flutter condition at $U_\infty = 22.5\,\text{m/s}$ (with speeds 4% and 8% higher than the body freedom flutter mode critical speeds of the frozen and lateral sloshing models, respectively) and $w_{g_a} = 0.2\,\text{m/s}$. The local angle of attack and the first mode responses are shown in Figure 14a,b comparing the four considered cases. The linear sloshing model leads to a flutter response with divergent

exponential envelope. The same occurs more slowly for the linear sloshing response. In contrast, vertical sloshing helps prevent the response from growing indefinitely, favoring the onset of limit cycle oscillations (LCOs). With regard to full sloshing, the oscillations are damped completely by vertical sloshing due to the additional margin of stability provided by lateral sloshing dynamics.

(a)

(b)

Figure 13. $U_\infty = 21.1\,\text{m/s}$ and $w_{g_a} = 0.2\,\text{m/s}$—Test Case 2. (**a**) Local angle of attack. (**b**) First structural mode.

(a)

Figure 14. *Cont.*

(b)
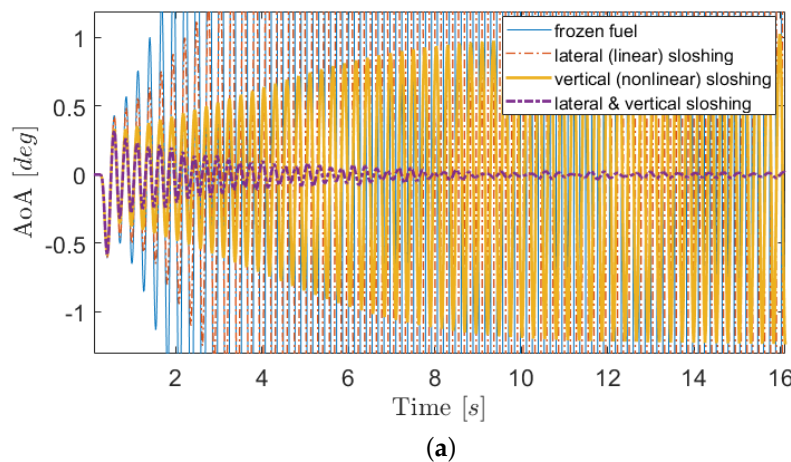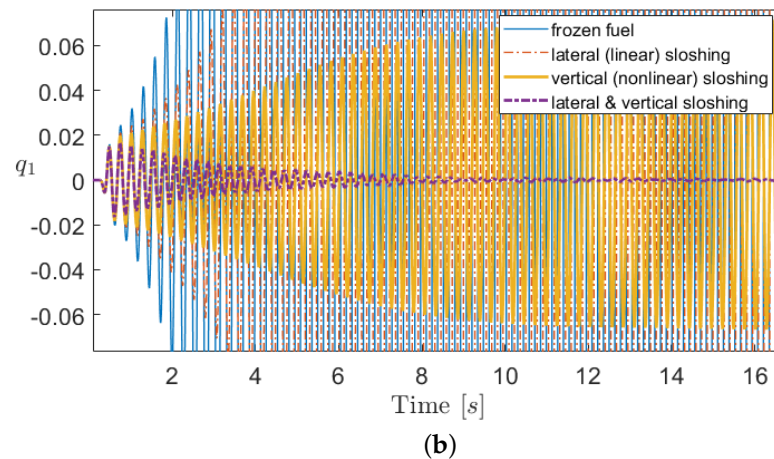
Figure 14. $U_\infty = 22.5\,\mathrm{m/s}$ and $w_{g_a} = 0.2\,\mathrm{m/s}$—Test Case 2. (**a**) Local angle of attack. (**b**) First structural mode.

5. Concluding Remarks

In this work, the effects of linear and nonlinear sloshing dynamics of fuel present inside the tanks were studied. Specifically, the investigation focused on the stability and response of a flexible flying wing model involving flight dynamics and aeroelasticity. The aircraft equations of motion were linearised around a stationary level-flight trim condition and recast in time-domain state-space form, thus obtaining an aeroelastic model that includes rigid-body, elastic, and aerodynamic states. Furthermore, the combined effects of linear and nonlinear sloshing dynamics were modelled by directly adding the two lateral and vertical contributions, respectively, to the aeroelastic system. Linear sloshing was described using an equivalent mechanical model (EMM) capable of restoring the actions exerted by the liquid following latero-rotational perturbations of the tank. Similar to the modeling of unsteady aerodynamics, the EMM introduced additional states related to liquid dynamics. Nonlinear vertical sloshing is a phenomenon caused by accelerations perpendicular to the liquid free surface. Rather than providing a coupling between the dynamics of the free surface and the rest of the system, it can instead be considered a kind of mechanical energy sink. Thus, vertical sloshing dynamics was modelled with a neural-network-based ROM driven by experimental data. Two case studies were considered; one with a single tank placed beneath the aircraft's center of mass, and the second with two tanks placed symmetrically underneath the wings. For the two case studies, the effects of sloshing dynamics on the stability and response were investigated by comparing cases where the liquid is assumed to be a frozen mass, and the other where the liquid is allowed to slosh freely. The results showed how linear sloshing dynamics can significantly influence aircraft stability as a result of their coupling with aeroelastic dynamics. Gust response analyses revealed that the performance of vertical sloshing provides additional damping in both pre-critical and post-critical conditions. Indeed, the presence of limit-cycle oscillations after the flutter guarantees an enhanced margin of stability for the system. The modeling presented herein will allow for the verification of the effects of sloshing on the stability and response of commercial aircraft, including next-generation configurations that may include large tanks within the fuselage. In addition, the high scalability of the presented sloshing reduced-order models will enable the usage of such models in the design phase of preliminary aircraft.

Author Contributions: Data curation, F.S.; Formal analysis, M.P.; Funding acquisition, F.M.; Investigation, F.S.; Methodology, M.P., F.S. and F.M.; Supervision, F.M.; Validation, F.M.; Writing – original draft, M.P. All authors have read and agreed to the published version of the manuscript.

Conflicts of Interest: The authors declare that they have no conflict of interest.

References

1. Gambioli, F.; Chamos, A.; Jones, S.; Guthrie, P.; Webb, J.; Levenhagen, J.; Behruzi, P.; Mastroddi, F.; Malan, A.; Longshaw, S.; et al. Sloshing Wing Dynamics-Project Overview Sloshing Wing Dynamics—Project Overview. In Proceedings of the 8th Transport Research Arena TRA 2020, Helsinki, Finland, 27–30 April 2020.
2. Firouz-Abadi, R.D.; Zarifian, P.; Haddadpour, H. Effect of Fuel Sloshing in the External Tank on the Flutter of Subsonic Wings. *J. Aerosp. Eng.* **2014**, *27*, 04014021.
3. Farhat, C.; Chiu, E.K.y.; Amsallem, D.; Schotté, J.S.; Ohayon, R. Modeling of Fuel Sloshing and its Physical Effects on Flutter. *AIAA J.* **2013**, *51*, 2252–2265.
4. Colella, M.; Saltari, F.; Pizzoli, M.; Mastroddi, F. Sloshing reduced-order models for aeroelastic analyses of innovative aircraft configurations. *Aerosp. Sci. Technol.* **2021**, *118*, 107075.
5. Pizzoli, M. Investigation of Sloshing Effects on Flexible Aircraft Stability and Response. *Aerotec. Missili Spaz.* **2020**, *99*, 297–308.
6. Abramson, H.N. *The Dynamic Behaviour of Liquids in Moving Containers with Applications to Space Vehicle Technology*; The National Aeronautics and Space Administration: Washington, DC, USA, 1966; p. 464.
7. Ibrahim, R. *Liquid Sloshing Dynamics: Theory and Applications*; EngineeringPro Collection; Cambridge University Press: Cambridge, UK, 2005.
8. Graham, E.; Rodriquez, A.M. *The Characteristics of Fuel Motion Which Affect Airplane Dynamics*; Technical Report; Douglas Aircraft Co. Inc., Defense Technical Information Center: Los Angeles, CA, USA, 1951.
9. Benjamin, T.B.; Ursell, F.J.; Taylor, G.I. The stability of the plane free surface of a liquid in vertical periodic motion. *Proc. R. Soc. London. Ser. A. Math. Phys. Sci.* **1954**, *225*, 505–515.
10. Wright, M.D.; Gambioli, F.; Malan, A.G. CFD Based Non-Dimensional Characterization of Energy Dissipation Due to Verticle Slosh. *Appl. Sci.* **2021**, *11*, 33.
11. Calderon-Sanchez, J.; Martinez-Carrascal, J.; Gonzalez-Gutierrez, L.M.; Colagrossi, A. A global analysis of a coupled violent vertical sloshing problem using an SPH methodology. *Eng. Appl. Comput. Fluid Mech.* **2021**, *15*, 865–888.
12. Marrone, S.; Colagrossi, A.; Gambioli, F.; González-Gutiérrez, L. Numerical study on the dissipation mechanisms in sloshing flows induced by violent and high-frequency accelerations. I. Theoretical formulation and numerical investigation. *Phys. Rev. Fluids* **2021**, *6*, 114801.
13. Marrone, S.; Colagrossi, A.; Calderon-Sanchez, J.; Martinez-Carrascal, J. Numerical study on the dissipation mechanisms in sloshing flows induced by violent and high-frequency accelerations. II. Comparison against experimental data. *Phys. Rev. Fluids* **2021**, *6*, 114802.
14. Titurus, B.; Cooper, J.E.; Saltari, F.; Mastroddi, F.; Gambioli, F. Analysis of a Sloshing Beam Experiment. In Proceedings of the International Forum on Aeroelasticity and Structural Dynamics, Savannah, GA, USA, 9–13 June 2019; Volume 139.
15. Wright, M.; Gambioli, F.; Malan, A.G. A Non-dimensional Characterization of Structural Vibration Induced Vertical Slosh. In Proceedings of the 31st International Ocean and Polar Engineering Conference, Rhodes, Greece, 20–25 June 2021;
16. Saltari, F.; Pizzoli, M.; Coppotelli, G.; Gambioli, F.; Cooper, J.E.; Mastroddi, F. Experimental characterisation of sloshing tank dissipative behaviour in vertical harmonic excitation. *J. Fluids Struct.* **2022**, *109*, 103478.
17. Constantin, L.; De Courcy, J.; Titurus, B.; Rendall, T.; Cooper, J. Sloshing induced damping across Froude numbers in a harmonically vertically excited system. *J. Sound Vib.* **2021**, *510*, 116302.
18. Liu, W.; Longshaw, S.M.; Skillen, A.; Emerson, D.R.; Valente, C.; Gambioli, F. A High-performance Open-source Solution for Multiphase Fluid-Structure Interaction. *Int. J. Offshore Polar Eng.* **2022**, *32*, 1–7.
19. Longshaw, S.M.; Liu, W.; Skillen, A.; Jones, B.W.; Malan, A.G.; Michel, J.; Marrone, S.; Gambioli, F. A Coupled FSI Framework Using the Multiscale Universal Interface. In Proceedings of the International Forum on Aeroelasticity and Structural Dynamics, Madrid, Spain, 13–17 June 2022.
20. Malan, A.G.; Jones, B.W.S.; Malan, L.C.; Wright, M. Accurate Prediction of Violent Slosh Loads via a Weakly Compressible VoF Formulation. In Proceedings of the 31st International Ocean and Polar Engineering Conference, Rhodes, Greece, 20–25 June 2021;
21. Jones, B.W.A.; Wright, M.D.; Malan, A.G.; Farao, J.; Gambioli, F.; Longshaw, S. A High Fidelity Fluid-Structure-Interaction Model of the Airbus Protospace Slosh Damping Experiment. In Proceedings of the International Forum on Aeroelasticity and Structural Dynamics 2022, Madrid, Spain, 13–17 June 2022.

22. Hall, J.; Rendall, T.; Allen, C.B. A Two-Dimensional Computational Model of Fuel Sloshing Effects on Aeroelastic Behaviour. In Proceedings of the 31st AIAA Applied Aerodynamics Conference, San Diego, CA, USA, 24–27 June 2013.

23. Courcy, J.J.D.; Constantin, L.; Titurus, B.; Rendall, T.; Cooper, J.E. Gust Loads Alleviation Using Sloshing Fuel. In Proceedings of the AIAA Scitech 2021 Forum, Online, 11–15 & 19–21 January 2021.

24. Pizzoli, M.; Saltari, F.; Mastroddi, F.; Martinez-Carrascal, J.; González-Gutiérrez, L.M. Nonlinear reduced-order model for vertical sloshing by employing neural networks. *Nonlinear Dyn.* **2021**, *107*, 1469–1478.

25. Saltari, F.; Pizzoli, M.; Gambioli, F.; Jetzschmann, C.; Mastroddi, F. Sloshing reduced-order model based on neural networks for aeroelastic analyses. *Aerosp. Sci. Technol.* **2022**, *127*, 107708.

26. Haykin, S.O. *Neural Networks and Learning Machines*, 3nd ed.; Pearson: London, UK, 2009.

27. Saltari, F.; Riso, C.; Matteis, G.D.; Mastroddi, F. Finite-Element-Based Modeling for Flight Dynamics and Aeroelasticity of Flexible Aircraft. *J. Aircr.* **2017**, *54*, 2350–2366.

28. Albano, E.; Rodden, W.P. *MSC/NASTRAN Aeroelastic Analysis' User's Guide*; MSC Software: Newport Beach, CA, USA, 1994.

29. Morino, L.; Mastroddi, F.; Troia, R.D.; Ghiringhelli, G.L.; Mantegazza, P. Matrix fraction approach for finite-state aerodynamic modeling. *AIAA J.* **1995**, *33*, 703–711.

30. Burnett, E.; Atkinson, C.; Beranek, J.; Sibbitt, B.; Holm-Hansen, B.; Nicolai, L. NDOF Simulation Model for Flight Control Development with Flight Test Correlation. In Proceedings of the AIAA Modeling and Simulation Technologies Conference, Toronto, ON, Canada, 2–5 August 20102010; pp. 2010–7780.

31. Schmidt, D. Stability augmentation and active flutter suppression of a flexible flying-wing drone. *J. Guid. Control. Dyn.* **2016**, *39*, 409–422.

32. Saltari, F.; Traini, A.; Gambioli, F.; Mastroddi, F. A linearized reduced-order model approach for sloshing to be used for aerospace design. *Aerosp. Sci. Technol.* **2021**, *108*, 106369.

33. Pizzoli, M.; Saltari, F.; Coppotelli, G.; Mastroddi, F. Experimental Validation of Neural-Network-Based Nonlinear Reduced-Order Model for Vertical Sloshing. In Proceedings of the AIAA Scitech 2022 Forum, San Diego, CA, USA & Virtual, 3–7 January 2022.